Charge solitons and their dynamical mass in one-dimensional arrays of Josephson junctions

Jens Homfeld,[1] Ivan Protopopov,[2,3] Stephan Rachel,[4] and Alexander Shnirman[1,5]

[1]*Institut für Theorie der Kondensierten Materie, Karlsruhe Institute of Technology, D-76128 Karlsruhe, Germany*

[2]*Institut für Nanotechnologie, Karlsruhe Institute of Technology, D-76021 Karlsruhe, Germany*

[3]*Landau Institute for Theoretical Physics, RU-119334 Moscow, Russia*

[4]*Department of Physics, Yale University, New Haven, Connecticut 06520, USA*

[5]*DFG Center for Functional Nanostructures (CFN), Karlsruhe Institute of Technology, D-76128 Karlsruhe, Germany*

(Received 31 August 2010; revised manuscript received 20 December 2010; published 28 February 2011)

We investigate charge transport in one-dimensional arrays of Josephson junctions. In the interesting regime of "small charge solitons" (polarons), $\Lambda E_J > E_C > E_J$, where Λ is the (electrostatic) screening length, the charge dynamics are strongly influenced by the polaronic effects (i.e., by dressing of a Cooper pair by charge dipoles). In particular, the soliton's mass in this regime scales approximately as E_J^{-2}. We employ two theoretical techniques: the many-body tight-binding approach and the mean-field approach, and the results of the two approaches agree in the regime of "small charge solitons." Renormalization of the soliton's mass could be observed; for example, as enhancement of the persistent current in a ring-shaped array.

DOI: 10.1103/PhysRevB.83.064517 PACS number(s): 74.81.Fa, 85.25.Cp, 03.75.Lm, 05.45.Yv

I. INTRODUCTION

The physics of one- and two-dimensional arrays of Josephson junctions is surprisingly rich. Both one-dimensional (1-D)[1–9] and two-dimensional (2-D)[10–14] arrays (including granulated superconducting films) have been extensively investigated. Yet, many unanswered questions remain. In particular, the transport properties of 1-D arrays of Josephson junctions (JJs) are still not fully understood. Experiments[4,7,8] show various phenomena related to superconductor-insulator transitions, the Coulomb blockade, hysteresis, mixed Josephson-quasiparticle effects, etc. One of the challenging questions is the value and the origin of the mass of the charge carriers in the insulating regime. In the theoretical studies of Hermon *et al.*[5] it was shown that, if the grains have a large kinetic (or geometric) inductance, the system's dynamics are governed by the sine-Gordon model and, therefore, kink-like topological excitations (i.e., charge solitons) are the charge carriers. Thus, one could expect the characteristics of the array (i.e., the current-voltage characteristics), to be dual to those of the discrete arrays with parallel coupling of Josephson junctions (see, e.g., Ref. 16), where fluxons (flux solitons) are responsible for transport. In Ref. 9 the domain of applicability of this sine-Gordon description for charge solitons was analyzed. Simultaneous experiments by Haviland and Delsing[4] demonstrated the Coulomb blockade in 1-D arrays of JJs consistent with the existence of charge solitons. In the later experiments of Haviland's group,[7,8] considerable hysteresis in the I-V characteristic of the array was observed and attributed to a very large kinetic inductance. The physical origin of this inductance remained unclear. A few years later, Zorin[15] pointed out that a current-biased small-capacitance JJ develops an inductive response on top of the capacitive response. This phenomenon was called Bloch inductance. A closely related inductive coupling between two charge qubit was studied in Ref. 17. The role of the Bloch inductance in Josephson arrays was studied in Ref. 15 for the case of an infinite screening length, that is, when the array serves as a zero-dimensional lumped circuit element.

In this paper we employ two complimentary techniques to study the charge propagation in infinite Josephson arrays with finite but large screening length. We consider arrays free of disorder. Specifically, we concentrate on calculating the effective mass of the charge carriers. Both approaches (i.e., the many-body tight-binding technique and the mean-field technique) agree for not-very-small ratios E_J/E_C. In particular, the effective mass of a charge soliton scales approximately as E_J^{-2} in this regime.

These results are sufficient to determine the amplitude of the persistent current in a ring-shaped array with exactly one extra Cooper pair and with no disorder (offset charges). We predict a considerable enhancement of the persistent current which should be experimentally observable. To describe the transport in more complicated setups (i.e., in an array which is voltage biased at its edges), one has to include the crucial effects of dissipation and disorder. We plan to do so in the future. Yet, our result about the reduction of the effective mass of the solitons is clearly relevant for the theory of charge transport. Indeed, the mobility of the charges should increase with decreasing effective mass. Thus, irrespective of the particular transport mechanism, one should expect a strong enhancement of the current (conductivity) with increasing E_J.

II. THE SYSTEM

The system under study is shown in Fig. 1. The Josephson junctions with capacitance C connect the superconducting grains to each other and each grain has a capacitance C_0 to the ground. Typical values are $C \sim 1$ fF and $C_0 \sim 5$–20 aF. The system is governed by the usual Hamiltonian consisting of the Coulomb charging energy (kinetic energy) and the Josephson tunneling (potential energy):

$$H = \frac{1}{2}\sum_{r,r'} U(r-r')n_r n_{r'} - E_J \sum_r \cos(\theta_r - \theta_{r-1}). \qquad (1)$$

Here, n_r are integer-valued island charges (in units of $2e$) and θ_r are the corresponding canonically conjugate phases,

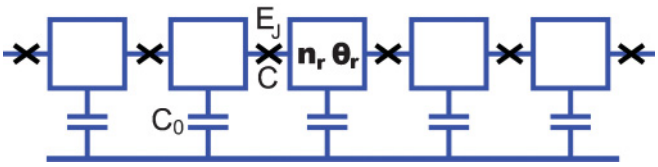

FIG. 1. (Color online) Array of Josephson junctions.

$[n_r, e^{i\theta_{r'}}] = e^{i\theta_r}\delta_{rr'}$. The matrix of Coulomb interactions $U(r)$ is given by

$$U(r) = 2E_C \int_{-\pi}^{\pi} \frac{dk}{2\pi} \frac{e^{ikr}}{\Lambda^{-2} - 2(\cos k - 1)}, \tag{2}$$

with $E_C \equiv (2e^2)/2C$ being the charging energy and $\Lambda \equiv \sqrt{C/C_0}$ the screening length, which determines the spatial extent of the Coulomb interaction. In this paper we consider $\Lambda \gg 1$.

III. TIGHT-BINDING APPROACH

A. Qualitative discussion

In this section we explore the properties of Josephson arrays in the Coulomb blockade regime $E_J \ll E_C$. We consider the sector of Hilbert space with exactly one extra Cooper pair in the array. The simplest (and having minimal charging energy) representative of the unit-charge sector is the state in which the extra Cooper pair resides on some island R with all the other islands being neutral. The charging energy of such a state is given by $\mu_0 \equiv \frac{1}{2}U(0) \approx \Lambda E_C/2$. This is approximately the energy (rather high!) one has to invest to insert one Cooper pair into the array. Once the Cooper pair has been inserted it is free to move from one site to its neighbor via the hopping provided by the Josephson part of the Hamiltonian. In the limit of vanishingly small E_J only the simplest charge configurations described above are important, and we are led to the trivial tight-binding band $E(k) = -E_J \cos k$ for an extra Cooper pair in the Josephson chain (cf. Refs. 2 and 3).

The peculiarity of the 1-D Josephson chain, first noticed in Refs. 2 and 3 and used in Ref. 19, is that the simple picture sketched above is valid only for extremely small $E_J < E_C/\Lambda$. The reason is the presence of a large number of states lying at small energy $\sim E_C/\Lambda$ above the basic states (as opposed to much larger energy E_C which one might expect and which indeed happens in higher dimensions). One particular example is the charge configuration $|1,-1,1\rangle$ (Cooper pair and a properly oriented dipole nearby) having the energy $\frac{3}{2}U(0) - 2U(1) + U(2) \approx \mu_0 + E_C/\Lambda$. Thus, in the parameter range $\Lambda E_J > E_C > E_J$, called by the authors of Ref. 19 the small soliton regime, a Cooper pair inserted into the chain gets strongly dressed by virtual dipoles and the simplest tight-binding scheme breaks down. Dipole dressing was also mentioned in the context of transport in ion channels.[18]

In Ref. 19 the properties of the small charge solitons were addressed by successive inclusion of the charge configurations (up to 32 states) with larger and larger energies into the tight-binding scheme. A similar scheme was developed for polarons in Ref. 20. In this paper we construct a comprehensive description of the low-lying (with energies much smaller E_C) states in terms of a particular spin-$\frac{1}{2}$ model. We derive an effective Hamiltonian governing the model dynamics within the low-energy subspace. We then develop a tight-binding approach with an arbitrary number of the charge states taken into account.

B. Structure of the low-energy subspace

Let us first define more precisely what we mean under the low-lying states in the sector with total charge 1 and construct the complete classification of these states. Let us consider some charge configuration of size w. It is clear that the energy of such a configuration will certainly exceed E_C if $w > \Lambda$ (from now on we count energies from the energy μ_0 of a single Cooper pair). Thus, for the low-lying configurations $w < \Lambda$ we can expand the charging energy in powers of $1/\Lambda$ as

$$H_C = -\frac{E_C}{2}\sum_{rr'}|r-r'|n_r n_{r'} + \frac{E_C}{4\Lambda}\sum_{r,r'}(r-r')^2 n_r n_{r'} + \cdots. \tag{3}$$

We see that the typical charge configurations have large energy $\sim E_C \gg E_J$ and are not important for the low-energy physics. The exceptions are the states nullifying the first term in Eq. (3) and having the energy $\sim w E_C/\Lambda$. Note that the first term of the expansion (3) cannot take negative values, or there would exist configurations with electrostatic energy smaller than μ_0. As long as $w < \Lambda E_J/E_C$ these charge configurations hybridize effectively with the basic one leading to the formation of the small charge soliton. Thus, the condition

$$\sum_{rr'}|r-r'|n_r n_{r'} = 0 \tag{4}$$

is the mathematical definition of the low-energy subspace in the unit charge sector (we also call it the proper space). It can be shown (Appendix A) that the subspace (4) consists of all the configurations with two properties: (a) all the islands' charges n_r equal ± 1 or 0 and (b) any two charged islands separated by an arbitrary number of neutral islands have opposite charges. For example, the configurations $|1,0,-1,1\rangle$ and $|1,0,-1,0,1\rangle$ belong to the low-energy space while the configurations $|2,0,-1\rangle$ and $|1,0,1,0,-1\rangle$ do not. To describe the proper subspace in a clearer way, let us introduce variables σ_r defined on the links of the chain (the link r is the link connecting islands r and $r+1$):

$$\sigma_r^z = -\sum_{r'\geqslant r+1} n_{r'} + \sum_{r'\leqslant r} n_{r'}, \quad n_r = \frac{1}{2}\left(\sigma_r^z - \sigma_{r-1}^z\right). \tag{5}$$

The connection between variables σ_r^z and charges n_r for two configurations in the low-energy subspace is illustrated in Fig. 2. From the definition of σ_r^z and the properties of the states in the low-energy subspace one immediately concludes that the low-energy configurations are described by $\sigma_r^z = \pm 1$ for all r, that is, the low-energy subspace is isomorphic to the space of states for a spin-$\frac{1}{2}$ chain with σ_r^z being the z projections of the spins.

Due to the constraint $\sum_r n_r = 1$ the variable σ_r^z satisfies the boundary conditions

$$\sigma^z_{r\to-\infty} = -1, \quad \sigma^z_{r\to+\infty} = 1. \tag{6}$$

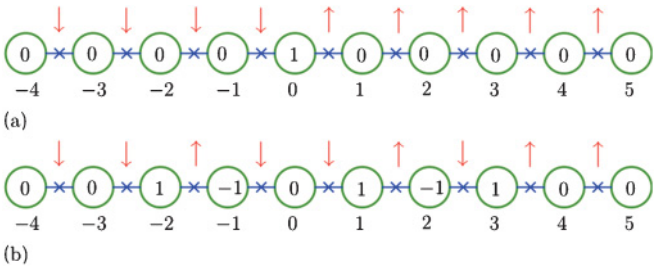

FIG. 2. (Color online) Connection between σ_r^z (defined on the links) and the charges of the islands n_r. In the low-energy subspace, σ_r^z can take only the two values ± 1 and are z projections of a spin $\frac{1}{2}$. (a) Basic charge configuration with only one charged island corresponds to an abrupt domain wall in terms of σ_r^z. (b) More complicated charge configuration (two additional dipoles) corresponding to a domain wall of finite thickness in the spin language.

Thus, an extra Cooper pair in the chain is described by a domain wall in the spin language.

C. Projecting the Hamiltonian

Having understood the structure of the low-energy space of the model we can project the full Hamiltonian (1) onto the proper subspace. The projection is carried out by noting that Cooper-pair tunneling between two neighboring islands corresponds to the spin flip in the link between them. Thus, the Josephson part of the Hamiltonian is given by

$$H_J = -E_J \sum_r \sigma_r^x. \tag{7}$$

Rewriting the charging energy in terms of spin variables we arrive at

$$H = \frac{1}{8}\sum_{r,r'} \left(\sigma_r^z - \sigma_{r-1}^z\right)\left(\sigma_{r'}^z - \sigma_{r'-1}^z\right) U(r-r') - E_J \sum_r \sigma_r^x. \tag{8}$$

To determine the spectrum of the single-charge sector of the Hamiltonian (8) we impose the boundary conditions (6) indicating the presence of a domain wall.

The Hamiltonian (8) takes into account the low-energy charge configurations of arbitrary width w. We understand, however, that the configurations with $w \gg \Lambda E_J/E_C$ are not important at low energies. Thus, we can further reduce the phase space by dropping out all the configurations of width w larger than some w_0. We expect that, at $w_0 \gg \Lambda E_J/E_C$, the resulting low-energy states are independent of w_0 and approximate correctly those of Hamiltonian (8).

Any state containing a domain wall of width less than w_0 is completely specified by the position R of the first spin up (which we call the coordinate of the charge soliton or domain wall) and the values of the z projections of the next w_0 spins $\{\tilde{\sigma}_1, \ldots, \tilde{\sigma}_{w_0}\}$. Given the state

$$|R\rangle|\tilde{\sigma}_1, \ldots, \tilde{\sigma}_{w_0}\rangle, \tag{9}$$

one can reconstruct the z projections of all spins in the chain according to

$$\sigma_r^z = \begin{cases} -1, & r < R \\ 1, & r = R \\ \tilde{\sigma}_{r-R}, & R+1 \leqslant r \leqslant R+w_0 \\ 1, & r > R+w_0. \end{cases} \tag{10}$$

For example, if we choose $w_0 = 5$, the states shown in Figs. 2(a) and 2(b) can be written as

$$|R=0\rangle|\uparrow,\uparrow,\uparrow,\uparrow,\uparrow\rangle, \tag{11}$$

$$|R=-2\rangle|\downarrow,\downarrow,\uparrow,\downarrow,\uparrow\rangle. \tag{12}$$

In Appendix B we describe how to project the Hamiltonian (8) onto the space of configurations with sizes less than or equal to w_0. We also perform a transition from the coordinates $|R\rangle$ to the quasimomentum k. The result reads

$$H = H_C - E_J \sum_{r=1}^{w_0} \sigma_r^x - E_J \left[\sum_{r=1}^{w_0} e^{irk} \left(T^\dagger \sigma_1^+\right)^r \sigma_r^- + e^{i(w_0+1)k} \prod_{r=1}^{w_0} \sigma_r^+ + \text{H.c.}\right], \tag{13}$$

where T is the operator of the right cyclic shift defined by $T|\tilde{\sigma}_1, \ldots, \tilde{\sigma}_{w_0}\rangle = |\tilde{\sigma}_{w_0}, \tilde{\sigma}_1, \ldots, \tilde{\sigma}_2\rangle$.

The Hamiltonian (13) constitutes the main result of this section. For $w_0 = 1, 2, \ldots, 5$ it can be shown to produce results equivalent to that of Ref. 19. Equation (13) reduces the initial many-body problem to a finite-dimensional Hamiltonian, readily accessible to numerics as long as not-too-large ($w_0 \leqslant 20$) charge configurations are important. In the next sections we present the results of numerical analysis of the Hamiltonian (13) and compare the results to those of the mean-field approach.

D. Results of the tight-binding approach

An example of the band structure obtained within the tight-binding approach is shown in Fig. 3. In Fig. 4 the two lowest bands are shown. We observe that the lowest band is parabolic for small momenta k and flattens in the outer

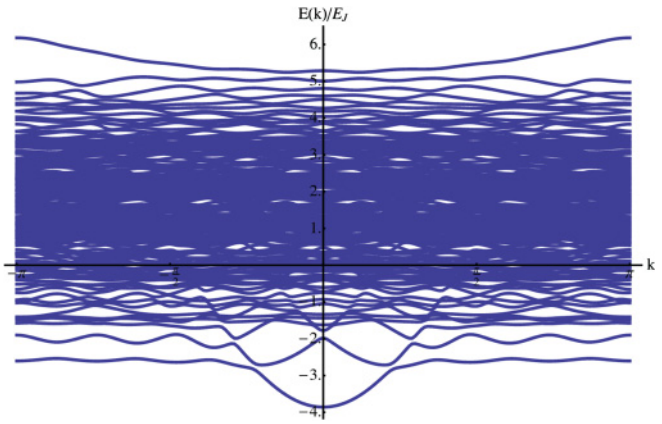

FIG. 3. (Color online) Spectrum of the tight-binding Hamiltonian (13) for $E_J/E_C = 0.4$ and $\Lambda = 10$. The number of charge states taken into account is 2^7.

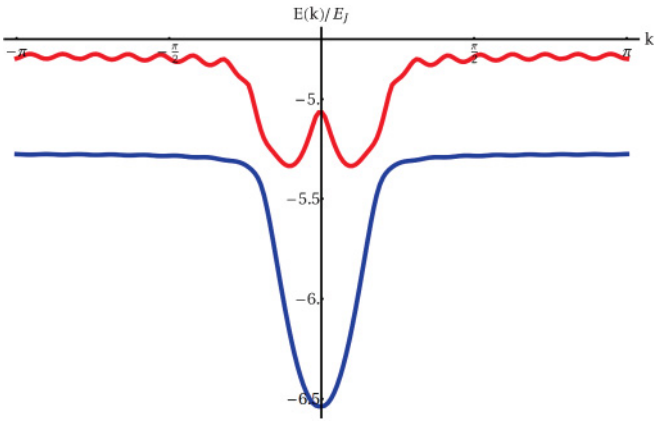

FIG. 4. (Color online) Two lowest energy bands for $\Lambda = 10$ and $E_J/E_C = 0.4$. The number of charge states taken into account is 2^{18}.

part of the Brillouin zone. This phenomenon was already observed in Ref. 19. To further emphasize the dispersion relation of the lowest band in Fig. 5 we show the group velocity of the soliton (dressed Cooper pair) as compared to the group velocity of an undressed Cooper pair. We find that the flattening of the dispersion relation in the outer region of the Brillouin zone leads to zero group velocity. In this paper we concentrate mostly on the investigation of the effective mass of the charge carriers. In the tight-binding approach we define $m_{\rm TB} = \hbar^2(\frac{\partial^2 E_0(k)}{\partial k^2}|_{k=0})^{-1}$, where $E_0(k)$ is the dispersion of the lowest band (ground state). In what follows we will compare this mass with the results of the mean-field theory.

1. Persistent current

As a first obvious application of our results, consider a ring-shaped array of N junctions with exactly one extra Cooper pair in it. If an external magnetic flux $\Phi_{\rm ext}$ is applied a persistent current will emerge. The periodic boundary condition for the

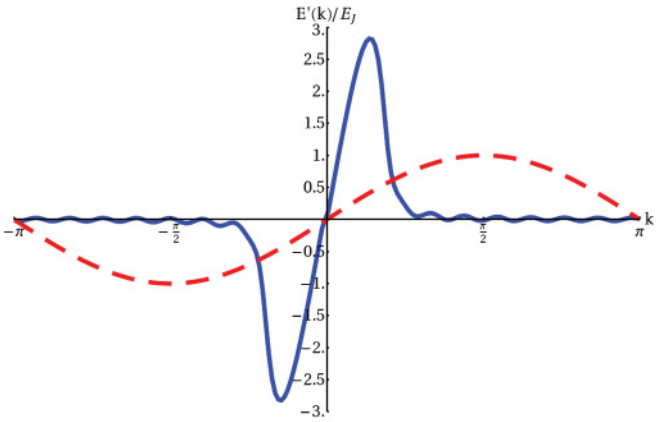

FIG. 5. (Color online) Solid (blue) line: the group velocity corresponding to the lowest energy band of Fig. 4. Dashed (red) line: the naive tight-binding group velocity with no dressing by dipoles taken into account.

Bloch wave with wave vector k reads

$$e^{ikN} = e^{2\pi \frac{\Phi_{\rm ext}}{\Phi_0}}. \tag{14}$$

Thus, as the external flux varies between $-\Phi_0/2$ and $\Phi_0/2$, the relevant wave vector varies between $-\pi/N$ and π/N. For large enough N the interval $[-\pi/N,\pi/N]$ is safely within the domain of the parabolic dispersion relation. Thus, we use the effective mass approximation and obtain, for the persistent current in the interval $\Phi_{\rm ext} \in [-\Phi_0/2,\Phi_0/2]$,

$$I(\Phi_{\rm ext}) \approx \frac{2e}{N}\frac{\hbar k}{m_{\rm eff}} = \frac{2e}{N^2 m_{\rm eff}}\frac{2\pi\hbar\Phi_{\rm ext}}{\Phi_0}, \tag{15}$$

where $m_{\rm eff}$ is the effective mass of the charge carrier (in the tight-binding approach we obtained $m_{\rm eff} = m_{\rm TB}$). Thus, the amplitude of the persistent current oscillations is given by

$$I_0 = \frac{2\pi\hbar e}{N^2 m_{\rm eff}}. \tag{16}$$

With no polaronic effects taken into account (i.e., for a bare Cooper pair) we would have $E_0^{\rm bare}(k) = -E_J\cos k$ and $m_{\rm eff}^{\rm bare} = \hbar^2/E_J$. Thus, we obtain

$$I_0 = \frac{2\pi e E_J}{\hbar N^2}\frac{m_{\rm eff}^{\rm bare}}{m_{\rm eff}} = \frac{\pi I_c}{N^2}\frac{m_{\rm eff}^{\rm bare}}{m_{\rm eff}}, \tag{17}$$

where I_c is the critical current of a single Josephson junction. We observe that the effective mass reduction via the polaronic effects enhances the persistent current. This effect should be experimentally observable.

IV. MEAN-FIELD THEORY

A. Description in terms of continuous polarization charges

An alternative description of the charge propagation in the array is given in terms of the continuous polarization charges; for example, the screening charges $q_n^{\rm gate}$ on the gate capacitances C_0 (see Fig. 6). For the system described in the previous section the continuous polarization charges are enslaved to the discrete charges n_r. That is, once a tunneling process occurs and the distribution n_r changes, the polarization charges adjust immediately to the new situation. To allow formally independent dynamics of polarization charges we introduce infinitesimal inductances L_0 as shown in Fig. (6). This leads to two independent degrees of freedom per cell of the array. One quantized charge degree of freedom $m_r = \sum_{k=r}^{\infty} n_k$ is the number of Cooper pairs that have tunneled through junction number r. Its conjugate phase is given by $\phi_r = \theta_r - \theta_{r-1}$ and the commutation relations read $[m_r, e^{i\phi_{r'}}] = e^{i\phi_r}\delta_{rr'}$. The second continuous-charge degree of freedom $Q_r \equiv \sum_{r'<r} q_{r'}^{\rm gate} + 2em_{-\infty}$ is equal to the polarization

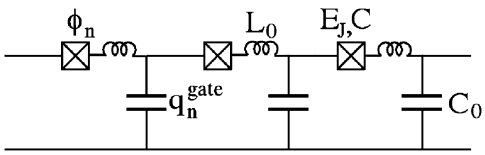

FIG. 6. Array of Josephson junctions with infinitesimal inductances L_0.

charge that has arrived at the junction number r or, alternatively, the integral of the displacement current flowing into junction r. The conjugate variable Φ_r is the magnetic flux on inductance L_0 in cell number r. The commutation relation reads $[\Phi_r, Q_{r'}] = i\hbar\delta_{rr'}$. We obtain the following Hamiltonian of the array:

$$H = \sum_r \left[\frac{(2em_r - Q_r)^2}{2C} - E_J \cos(\phi_r) + \frac{(Q_r - Q_{r-1})^2}{2C_0} + \frac{\Phi_r^2}{2L_0} \right]. \quad (18)$$

B. Mean-field approximation

The mean-field description is based on the Heisenberg equations of motion for the polarization charge Q_r following from (18):

$$L_0 \ddot{Q}_r = -\frac{1}{C}(Q_r - 2em_r) - \frac{2Q_r - Q_{r-1} - Q_{r+1}}{C_0}. \quad (19)$$

We average Eq. (19) over the state of the system and obtain

$$L_0 \langle \ddot{Q}_r \rangle = -V_r - \frac{2\langle Q_r \rangle - \langle Q_{r+1} \rangle - \langle Q_{r-1} \rangle}{C_0}, \quad (20)$$

where $V_r \equiv \langle \frac{1}{C}(Q_r - 2em_r) \rangle$ is the expectation value of the voltage drop across junction number r. In the mean-field approximation we calculate V_r by replacing the operators Q_r by their average values $\langle Q_r \rangle(t)$ in the Hamiltonian (18). Thus the problem factorizes to many single-junction problems. Each junction is governed by the Hamiltonian

$$H(Q(t)) = \frac{[2em - Q(t)]^2}{2C} - E_J \cos\phi, \quad (21)$$

where we have dropped the index r. The gate charge $Q(t)$ is a given function of time [to be replaced in each junction by $\langle Q_r \rangle(t)$]. For the expectation value of the voltage, we then obtain $V = \langle \partial_Q H \rangle$. The problem is now to find the quantum state of the junction in which the average $\langle \partial_Q H \rangle$ should be evaluated. We do so assuming that $\langle Q_r \rangle(t)$ is a slow function of time. This assumption should be checked for self-consistency later.

The Hamiltonian (21) possesses the (adiabatic) spectrum with discrete eigenvectors $|e_n(Q(t))\rangle$ obeying $\langle e_n \,|\, e_m \rangle = \delta_{nm}$ and eigenvalues $E_n(Q(t))$; cf. Fig. 7. The general wave function is a superposition $|\Psi(t)\rangle = \sum_n \alpha_n(t)|e_n(Q(t))\rangle$. Our

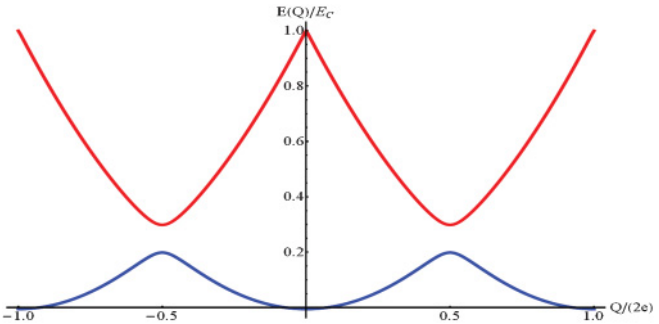

FIG. 7. (Color online) The ground and first-excited state E_0 and E_1, respectively, of (21).

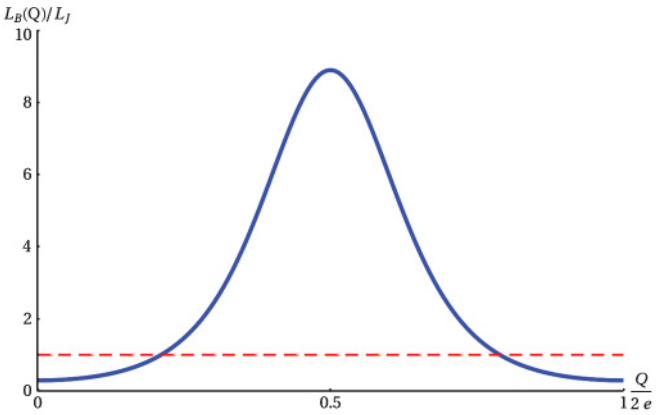

FIG. 8. (Color online) Solid line: Bloch inductance $L_B(Q)$ for $E_J/E_C = 0.5$, measured in units of the Josephson inductance L_J. Dashed line: $L_B(Q) = L_J$ for $E_J/E_C = \infty$.

aim is to determine $|\Psi(t)\rangle$ for a given function $Q(t)$. We restrict ourselves to the adiabatic case (i.e., we keep only terms of order $\ddot{Q}$ and $\dot{Q}^2$). After a calculation presented in Appendix C we arrive at

$$V = \langle \partial_Q H \rangle = \partial_Q E_0 + L_B \ddot{Q} + \tfrac{1}{2}(\partial_Q L_B)\dot{Q}^2. \quad (22)$$

Here we defined the Bloch inductance first introduced by Zorin:[15]

$$L_B = 2\hbar^2 \sum_{n>0} \frac{\langle e_n | \partial_Q H | e_0 \rangle^2}{(E_n - E_0)^3}. \quad (23)$$

[In Ref. 15 only the first excited state ($n = 1$) in (23) was taken into account and the contribution $\propto \partial_Q L_B$ in (22) was omitted.] For $E_J \ll E_C$ the Bloch inductance L_B is sharply peaked around $Q = e$ (see Fig. 8). In the opposite case, $E_J \gg E_C$, the Bloch inductance L_B is nearly constant, $L_B \approx L_J \equiv \frac{\Phi_0^2}{4\pi^2 E_J}$. Combining Eq. (22) and the self-consistency equation (20), we obtain

$$L_0 \ddot{Q}_r = -\left[\frac{2Q_r - Q_{r-1} - Q_{r+1}}{C_0} \right] - \left[\partial_Q E_0(Q_r) + L_B(Q_r)\ddot{Q}_r + \frac{1}{2}\partial_Q L_B(Q_r)\dot{Q}_r^2 \right], \quad (24)$$

where we substituted $\langle Q \rangle \to Q$ for clarity. We observe that the kinetic inductance is superseded by the Bloch inductance, at least around $Q = e$, and we can safely assume $L_0 \to 0$. Yet, in the regime $E_J \ll E_C$, when $L_B(Q)$ is exponentially small in the regions $Q \approx 0$ and $Q \approx 2e$, a finite geometric or kinetic inductance L_0 could be important. In the continuum limit (i.e., after the substitution $Q_{r+1} + Q_{r-1} - 2Q_r \to \partial_r^2 Q = Q''$), Eq. (24) reads

$$L_B(Q)\ddot{Q} - \frac{Q''}{C_0} + \frac{1}{2}(\partial_Q L_B)\dot{Q}^2 + \frac{\partial E_0(Q)}{\partial Q} = 0. \quad (25)$$

We now make the very important observation that (25) is the equation of motion for the following Lagrangian density:

$$\mathcal{L}(Q, \dot{Q}) = \frac{1}{2}L_B(Q)\dot{Q}^2 - \frac{1}{2C_0}Q'^2 - E_0(Q). \quad (26)$$

In the limit $E_J \gg E_C$, when $L_B \approx$ const and $E_0(Q) \propto \cos Q$ we obtain the usual sine-Gordon equation. On the other hand, in the limit $E_J \ll E_C$ Eq. (25) differs in several aspects from the sine-Gordon equation: (i) The first two terms of (25) describe a waveguide with a Q-dependent "light velocity" $c(Q) = [L_B(Q)C_0]^{-1/2}$. With the Bloch inductance having a peak value $L_{\max} = L_B(e)$ at $Q = e$ we obtain the minimal light velocity $c_{\min} = (L_{\max}C_0)^{-1/2}$. (ii) The ground-state energy E_0 is still a $2e$ periodic function of Q but it is no longer proportional to $\cos Q$. (iii) Since L_B depends strongly on Q, the third term of (25) is very important.

C. Solitonic solutions

We are now searching for a solitary wave traveling with velocity v by plugging the ansatz $Q(r - vt)$ into Eq. (25). This gives the following differential equation:

$$\frac{\partial}{\partial r}\left[\frac{1}{2}\left(L_B(Q)v^2 - \frac{1}{C_0}\right)Q'^2 + E_0(Q)\right] = 0. \quad (27)$$

Integrating we obtain

$$r - r_0 = \pm \int_{Q(r_0)}^{Q(r)} dQ \left[\frac{2C_0[E_0(Q) - E_{\min}]}{1 - L_B(Q)C_0v^2}\right]^{-1/2}. \quad (28)$$

Here, $E_{\min}$ is an integration constant and $\pm$ stands for the soliton or antisoliton solution, respectively. We impose the boundary conditions $Q(-\infty) = 0$ and $Q(+\infty) = 2e$ to describe the propagation of a single Cooper pair in the array. This also fixes the integration constant, $E_{\min} = E_0(0) = E_0(2e)$. The solitonic solutions only exist for $v \leqslant c_{\min}$.

D. Lorentz contraction

In the limit $E_J \gg E_C$, Eq. (25) reduces to the sine-Gordon equation and is Lorentz invariant. Thus solitons undergo the usual Lorentz contraction. In the other limit, $E_J \ll E_C$, Eq. (25) is not Lorentz invariant. The Lorentz contraction of the soliton takes a very peculiar shape. Consider a soliton moving with velocity v approaching $c_{\min}$ (we postpone for a moment a discussion on whether this is consistent with adiabaticity). For the center of the soliton, where $Q \approx e$, the relativistic regime is reached and it is Lorentz contracted (see Fig. 9). In contrast, the soliton's tails, where $Q \sim 0$ or $Q \sim 2e$, are unaffected by Lorentz contraction.

E. Rest energy and dynamical mass of the soliton

Using the Lagrangian density (26) we find the energy of a soliton:

$$E_{\rm sol}(v) = \frac{1}{C_0}\int_0^{2e} dQ \sqrt{\frac{2[E_0(Q) - E_0(0)]C_0}{1 - v^2L_B(Q)C_0}}. \quad (29)$$

For small velocities we expand and obtain $E_{\rm sol}(v) = E_{\rm rest} + \frac{1}{2}m_{\rm kin}v^2 + O(v^4)$. The rest energy of the soliton is given by

$$E_{\rm rest} = \int_0^{2e} dQ \sqrt{\frac{2[E_0(Q) - E_0(0)]}{C_0}}. \quad (30)$$

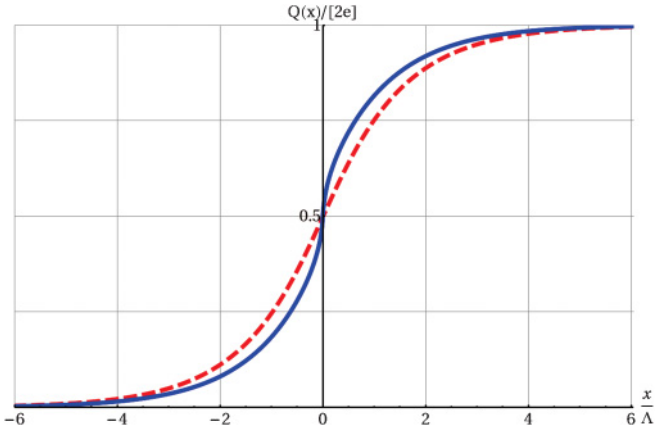

FIG. 9. (Color online) The solution $Q(x)$ from (28) for $v/c_{\min} = 0.1$ (red dashed curve) and $v/c_{\min} = 0.99$ (blue solid curve), both for $E_J/E_C = 0.5$.

For the kinetic mass we obtain

$$m_{\rm kin} = \int_0^{2e} dQ L_B(Q)\sqrt{2[E_0(Q) - E_0(0)]C_0}. \quad (31)$$

In the limit $E_J \gg E_C$, when $L_B \approx L_J =$ const, we obtain, as expected, the relativistic relation $E_{\rm rest} \approx m_{\rm kin}c_{\min}^2$ [in this limit the light velocity is Q-independent, $c(Q) \approx c_{\min} \approx (L_JC_0)^{-1/2}$].

In the opposite charging limit, $E_J \ll E_C$, no such relativistic relation exists. A simple estimate then gives

$$E_{\rm rest} \approx \Lambda\frac{E_C}{2}\left(1 - O\left[\frac{E_J}{E_C}\right]^2\right), \quad (32)$$

consistent with the result of Sec. III A. Note that the reduction of the soliton's rest energy with increasing E_J is consistent with the reduction of the Coulomb-blockade threshold observed in experiments.[8]

In the limit $E_J \ll E_C$ the Bloch inductance $L_B(Q)$ is sharply peaked around $Q = e$ and the integral of Eq. (31) is dominated by a small vicinity around this point. Here a two-state approximation is valid and gives $L_B = 2(\frac{E_C}{E_J})^2L_J\sin^5\theta$ with $\cot\theta \equiv (\frac{Q-e}{e})\frac{E_C}{E_J}$. As $L_B(Q)$ is sharply peaked around $Q = e$, we can replace $E_0(Q) - E_0(0)$ in (31) by its value at $Q = e$, $\frac{1}{4}E_C - \frac{1}{2}E_J$, leading to

$$m_{\rm kin} \approx m_{\rm kin}^{\rm bare}\frac{2E_C}{3\Lambda E_J}\left(1 - \frac{E_J}{E_C} + O\left[\frac{E_J}{E_C}\right]^2\right), \quad (33)$$

where $m_{\rm kin}^{\rm bare} \equiv \hbar^2/E_J$ is the "naive" tight-binding mass of a single Cooper pair. The polaronic reduction of the mass is evident from (33) in the regime $\Lambda E_J > E_C > E_J$.

F. Comparison with the tight-binding results

In Fig. 10 the mass $m_{\rm kin}$ obtained in the mean-field approach is compared with the mass $m_{\rm TB}$ from the tight-binding calculation. We observe a good correspondence for $E_J/E_C > 0.3$. This is the main result of this paper. The mass scales approximately as $\sim E_J^{-2}$. As the convergence of the tight-binding approach gets worse with increasing ratio $\frac{E_J}{E_C}$ we

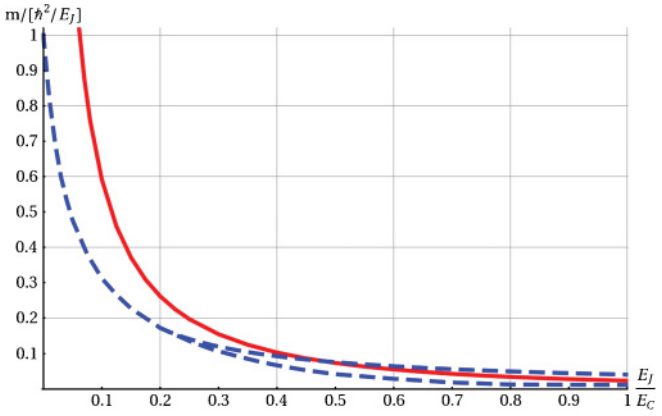

FIG. 10. (Color online) Solid (red) curve: mean-field mass $m_{\rm kin}$. Lower dashed (blue) curve: tight-binding mass m_{TB}. Upper dashed (blue) curve: upper boundary for m_{TB}.

also show the uncertainty of the result by giving the upper boundary for m_{TB} (upper dashed curve in Fig. 10).

G. Adiabaticity condition and the validity of the mean-field theory

The analysis above rests on two assumptions: (a) the dynamics of Q is slow and allows us to neglect the Landau-Zener tunneling in the derivation of Eq. (22) and (b) the field Q can be regarded as classical.

Since in terms of Q the solitons are large objects (with the size of the order of 2Λ) one can expect the second assumption to hold over a wide parameter range. In particular, at $E_J \sim E_C$ we can estimate the "effective Planck constant"[21] for the Lagrangian (26) as

$$\beta = \frac{2\pi\hbar}{(2e)^2}\sqrt{\frac{C_0}{L_B}} \sim \frac{1}{\Lambda}\sqrt{\frac{E_J}{E_C}} \ll 1. \tag{34}$$

While at small enough E_J/E_C strong suppression of the nonlinear Bloch inductance $L_B(Q)$ for $Q \neq e$ may become important, we expect this effect to be of minor significance in the intermediate range of E_J/E_C.

The situation with assumption (a) is much more tricky. First of all, the adiabaticity imposes an upper boundary for the velocity of solitons to be considered. In the limit $E_J \ll E_C$ the probability of a Landau-Zener transition into the first-excited level is given by

$$P = e^{-\frac{\pi}{2\hbar}\Delta^2\frac{1}{|\dot{\varepsilon}|}}, \tag{35}$$

where $\Delta \approx E_J$, and $\varepsilon(Q)$ is the difference of the charging energies of the two charge states involved in the process. Thus, $\dot{\varepsilon} = \dot{Q}\partial_Q\varepsilon$ and $|\partial_Q\varepsilon| \approx \frac{E_C}{2e}$. If we demand $P \leqslant e^{-x}$, the corresponding limitation on the soliton's velocity reads

$$v^2 \leqslant c_{\rm min}^2 \frac{1}{1+\left(\frac{2x}{\pi}\right)^2\frac{E_C}{E_J}}. \tag{36}$$

We see that, for $E_J/E_C \to 0$, the maximal velocity for which adiabaticity still holds goes to zero.

It is obvious that, even for a static soliton, the adiabaticity condition can be broken by fluctuations around the saddle point. Thus, the precise determination of the applicability region for the adiabatic approximation requires understanding of the characteristic time scale for the two-point correlation function of Q with the account of the nonlinear Bloch inductance. However, the good agreement between the mean-field theory and the tight-binding approach found in the calculation of the soliton mass for intermediate $E_J/E_C \sim 0.5$ allows us to expect that adiabaticity indeed holds in this parameter range for small soliton velocities.

V. CONCLUSIONS

In this paper we studied the dynamical properties of the charge carriers (charge solitons) in infinite one-dimensional Josephson arrays without disorder. We applied two complementary techniques and arrived at our main result: in the parameter regime $E_J < E_C < \Lambda E_J$ the polaronic effects strongly reduce the effective mass of the charge solitons which scales approximately as E_J^{-2}. This allowed us to make an experimentally relevant prediction about the enhancement of the persistent current in a ring-shaped array with one extra Cooper pair. Further studies of effects of disorder and dissipation are necessary to relate this results to transport experiments.

ACKNOWLEDGMENTS

We thank M. Berry, A. Ustinov, H. Rotzinger, and R. Schäfer for numerous fruitful discussions. IP acknowledges support from German-Israeli Foundation (GIF) and from Alexander von Humboldt Foundation. SR acknowledges support from the Deutsche Forschungsgmeinschaft (DFG) under Grant No. RA 1949/1-1.

APPENDIX A: LOW-LYING EXCITATIONS AND THE SPIN FORMULATION

The aim of the present appendix is to find an explicit description of the low-energy charge configurations satisfying the constraint

$$\sum_{rr'} |r-r'|n_r n_{r'} = 0. \tag{A1}$$

Let us consider one such configuration. We try to add a dipole at islands R and $R+1$ to this configuration; that is, we construct a new configuration given by

$$\tilde{n}_r = n_r + \delta_{rR} - \delta_{r,R+1}. \tag{A2}$$

For the new configuration to belong to the low-lying sector we need the following condition to hold:

$$\sum_{rr'} |r-r'|\tilde{n}_r\tilde{n}_{r'} = 2\sum_r n_r(|r-R| - |r-R-1|) - 2 = 0. \tag{A3}$$

We can rewrite this condition as

$$\sum_{r\geqslant R+1} n_r - \sum_{r\leqslant R} n_r = 1. \tag{A4}$$

In terms of the spin variable σ_r^z introduced in Sec. III B, Eq. (A4) is equivalent to the condition $\sigma_R^z = -1$. After the

creation of an additional dipole (i.e., the Cooper pair tunneling from island $R+1$ to island R) the new state is described by

$$\tilde{\sigma}_r^z = -\sum_{r'\geqslant r+1} \tilde{n}_{r'} + \sum_{r'\leqslant r} \tilde{n}_{r'} = \sigma_r^z + 2\delta_{r,R}. \tag{A5}$$

We thus conclude that the Cooper pair tunneling from island $R+1$ to island R is allowed (i.e., drives the system into another state within the low-energy subspace) if $\sigma_R^z = -1$. Such a tunneling corresponds to the spin flip at the link connecting islands R and $R+1$. It is easy to check that the inverse process (tunneling from R to $R+1$) is allowed only when $\sigma_R^z = 1$ and also leads to the flip of σ_R^z. Taking into account that a single Cooper pair at island R is described in terms of σ_r^z by a domain wall

$$\sigma_{r<R}^z = -1, \quad \sigma_{r\leqslant R}^z = 1, \tag{A6}$$

we conclude that the low-energy configurations are those with $\sigma_r^z = \pm 1$ for all r. Translated into the charge language this condition gives the conditions mentioned in the main text (Sec. III B).

APPENDIX B: PROJECTING THE HAMILTONIAN

We consider the action of the Josephson term in the Hamiltonian (8) on state (9). Obviously, we can drop all the terms with $r > R+w_0$ or $r < R-w_0-1$ from the sum over r since, acting on state (9), they inevitably create the configuration of width greater than w_0. The terms σ_r^x with $R+1 \leqslant r \leqslant R+w_0$ do not change the position of the first spin up in the chain and, thus, the coordinate of the soliton R. Thus, their action is described by

$$\sum_{r=R+1}^{R+w_0} \sigma_r^x |R\rangle|\tilde{\sigma}_1, \ldots, \tilde{\sigma}_{w_0}\rangle = |R\rangle \sum_{i=1}^{w_0} \tilde{\sigma}_i^x |\, \tilde{\sigma}_1, \ldots, \tilde{\sigma}_{w_0}\rangle\,. \tag{B1}$$

We consider now the action of σ_R^x. It is convenient to introduce the operator of the right cyclic shift T acting on the states $|\tilde{\sigma}_1, \ldots, \tilde{\sigma}_{w_0}\rangle$ according to

$$T|\tilde{\sigma}_1, \ldots, \tilde{\sigma}_{w_0}\rangle = |\, \tilde{\sigma}_{w_0}, \tilde{\sigma}_1, \ldots, \tilde{\sigma}_2\rangle\,. \tag{B2}$$

Assume that, in the state $|\tilde{\sigma}_1, \ldots, \tilde{\sigma}_{w_0}\rangle$, exactly k first spins are down (-1) (we require now $0 \leqslant k \leqslant w_0 - 1$; the case of w_0 spins down will be considered separately). The direction of other spins is arbitrary. In this case the action of σ_R^x on our state is given by

$$\sigma_R^x |R\rangle|\tilde{\sigma}_1, \ldots, \tilde{\sigma}_{w_0}\rangle = |R+k+1\rangle [T^+]^{k+1} \left[\prod_{j=1}^{k+1} \tilde{\sigma}_j^+\right] \tilde{\sigma}_{k+1}^- |\tilde{\sigma}_1, \ldots, \tilde{\sigma}_{w_0}\rangle. \tag{B3}$$

On the other hand, if in the given state exactly $m \neq k$ first spins are -1, then

$$\left[\prod_{j=1}^{k+1} \tilde{\sigma}_j^+\right] \tilde{\sigma}_{k+1}^- |\tilde{\sigma}_1, \ldots, \tilde{\sigma}_{w_0}\rangle = 0. \tag{B4}$$

Thus we conclude that, for any state (except the state with all spins down),

$$\sigma_R^x |R\rangle|\tilde{\sigma}_1, \ldots, \tilde{\sigma}_{w_0}\rangle = \sum_{k=0}^{w_0-1} |R+k+1\rangle [T^+]^{k+1} \left[\prod_{j=1}^{k+1} \tilde{\sigma}_j^+\right] \tilde{\sigma}_{k+1}^- |\tilde{\sigma}_1, \ldots, \tilde{\sigma}_{w_0}\rangle. \tag{B5}$$

Finally, taking into account that

$$\sigma_R^x |R\rangle|\downarrow, \ldots, \downarrow\rangle = |R+w_0+1\rangle \left[\prod_{j=1}^{w_0} \tilde{\sigma}_j^+\right] |\downarrow, \ldots, \downarrow\rangle, \tag{B6}$$

we find for the projection of σ_R^x onto the space spanned by the configurations of width less than or equal to w_0:

$$\sigma_R^x |R\rangle|\tilde{\sigma}_1, \ldots, \tilde{\sigma}_{w_0}\rangle = \left[\sum_{k=1}^{w_0} |R+k\rangle [T^+]^k \left[\prod_{j=1}^{k} \tilde{\sigma}_j^+\right] \tilde{\sigma}_k^- + |R+w_0+1\rangle \left[\prod_{j=1}^{w_0} \tilde{\sigma}_j^+\right]\right] |\tilde{\sigma}_1, \ldots, \tilde{\sigma}_{w_0}\rangle. \tag{B7}$$

The last part of the Josephson Hamiltonian

$$\sum_{r=R-1}^{R-w-1} \sigma_r^x, \tag{B8}$$

after the projection onto the subspace of interest, produces an expression conjugate to (B7). Thus, summing up all the contributions, we find the projected Josephson Hamiltonian:

$$\begin{aligned} H_J |R\rangle|\tilde{\sigma}_1, \ldots, \tilde{\sigma}_{w_0}\rangle = {} & -E_J |R\rangle \sum_{k=1}^{w_0} \tilde{\sigma}_k^x |\tilde{\sigma}_1, \ldots, \tilde{\sigma}_{w_0}\rangle \\ & -E_J \left[\sum_{k=1}^{w_0} |R+k\rangle [T^+]^k \left[\prod_{j=1}^{k} \tilde{\sigma}_j^+\right] \tilde{\sigma}_k^- + |R+w_0+1\rangle \left[\prod_{j=1}^{w_0} \tilde{\sigma}_j^+\right] + \text{H.c.}\right] \\ & \times |\tilde{\sigma}_1, \ldots, \tilde{\sigma}_{w_0}\rangle. \end{aligned} \tag{B9}$$

Going to the momentum domain with respect to the cyclic coordinate R and performing some simplifications based on the elementary properties of T and $\tilde{\sigma}_k^{\pm}$, we finally arrive at Eq. (13).

APPENDIX C: ADIABATIC CALCULATION

Here we use a technique proposed by Berry[22] where we apply several unitary transformations, so that the eigenstates of the transformed Hamiltonians approach asymptotically the actual evolving state.

We consider the adiabatic case and the terms of orders higher than $\dot{Q}$ and $\dot{Q}^2$ are omitted. The general transformation reads

$$H_{k+1}(t) = U_k^\dagger H_k U_k - i\hbar U_k^\dagger \dot{U}_k, \tag{C1}$$

with $U_k(t)$ being the time-dependent unitary operator that diagonalizes H_k at each time t. We can write

$$\left|e_n^{(k)}(t)\right\rangle = U_k(t)\,|n\rangle\,, \tag{C2}$$

where $|e_n^{(k)}(t)\rangle$ are the eigenvectors satisfying

$$H_k(t)\left|e_n^{(k)}(t)\right\rangle = E_n^{(k)}(t)\left|e_n^{(k)}(t)\right\rangle, \tag{C3}$$

and time-independent vectors $|n\rangle$ can be chosen arbitrarily; for example, $|n\rangle = |e_n^{(0)}(t=-\infty)\rangle$. We now perform the first step of this process explicitly. As Hamiltonian $H_0(t)$ we take (21) with $|e_n^{(0)}(t)\rangle = |e_n(Q(t))\rangle$. From (C2) we find

$$U_0(t) = \sum_n \left|e_n^{(0)}(t)\right\rangle\langle n|\,. \tag{C4}$$

Applying (C1) gives the transformed Hamiltonian

$$H_1(t) = \sum_n |n\rangle\langle n|E_n^{(0)} - i\hbar \sum_{\substack{m,n \\ m\neq n}} |n\rangle\langle e_n^{(0)}\,|\,\dot{e}_m^{(0)}\rangle\langle m|. \tag{C5}$$

We find $|e_n^{(1)}(t)\rangle$ by applying the usual time-independent perturbation theory with the perturbation being the second term on the right-hand side of (C5). This gives the new transformation matrix $U_1(t)$ because $|e_n^{(1)}(t)\rangle = U_1(t)|n\rangle$, which can be used for a second transformation to obtain $H_2(t)$ with eigenvectors $|e_n^{(2)}(t)\rangle$. After calculating $|e_n^{(2)}(t)\rangle$ we can go back to the desired $|e_n^{(0)}(t)\rangle \equiv |e_n\rangle$ basis via

$$|\Psi(t)\rangle = U_0(t)U_1(t)\left|e_n^{(2)}(t)\right\rangle. \tag{C6}$$

Putting everything together gives

$$|\Psi(t)\rangle = |e_n\rangle\left[1 - \frac{1}{2}\sum_{m\neq n}\frac{f_{mn}^2(t)}{\Omega_{mn}^2(t)}\right] + \sum_{m\neq n}|e_m\rangle \times \left[\frac{f_{mn}}{i\Omega_{mn}} - \sum_{k\neq n}\frac{f_{mk}f_{kn}}{\Omega_{mn}\Omega_{kn}} + \frac{\dot{f}_{mn}}{\Omega_{mn}^2} - \frac{f_{mn}}{\Omega_{mn}^3}\frac{\partial\Omega_{mn}}{\partial Q}\dot{Q}\right] \tag{C7}$$

with $f_{nm} \equiv \dot{Q}\langle\partial_Q e_n\,|\,e_m\rangle$ and $\Omega_{nm} \equiv \frac{E_n - E_m}{\hbar}$. We are now able to calculate the voltage V_r with $|\Psi(t)\rangle$, where we set $n = 0$ in (C7) as we consider our system being initially in the ground state. We use $\langle e_n\,|\,\partial_Q H\,|\,e_m\rangle = \hbar\Omega_{nm}\langle\partial_Q e_n\,|\,e_m\rangle\, for\, n \neq m$ and $e_n\,|\,\partial_Q H\,|\,e_n\rangle = \partial_Q E_n$ and arrive at Eqs. (22) and (23).

[1] R. M. Bradley and S. Doniach, Phys. Rev. B **30**, 1138 (1984).
[2] A. A. Odintsov, JETP Lett. **60**, 738 (1994).
[3] A. A. Odintsov, Phys. Rev. B **54**, 1228 (1996).
[4] D. B. Haviland and P. Delsing, Phys. Rev. B**54**, R6857 (1996).
[5] Z. Hermon, E. Ben-Jacob, and G. Schön, Phys. Rev. B **54**, 1234 (1996).
[6] L. I. Glazman and A. I. Larkin, Phys. Rev. Lett. **79**, 3736 (1997).
[7] D. B. Haviland, K. Andersson, and P. Ågren, J. Low Temp. Phys. **118**, 733 (2000).
[8] P. Ågren, K. Andersson, and D. B. Haviland, J. Low Temp. Phys. **124**, 291 (2001).
[9] V. Gurarie and A. Tsvelik, J. Low Temp. Phys. **135**, 245 (2004).
[10] K. B. Efetov, Sov. Phys. JETP **51**, 1015 (1980).
[11] J. E. Mooij, B. J. van Wees, L. J. Geerligs, M. Peters, R. Fazio, and G. Schön, Phys. Rev. Lett. **65**, 645 (1990).
[12] M. P. A. Fisher, Phys. Rev. Lett. **65**, 923 (1990).
[13] R. Fazio and G. Schön, Phys. Rev. B **43**, 5307 (1991).
[14] R. Fazio and H. van der Zant, Phys. Rep. **355**, 235 (2001).
[15] A. B. Zorin, Phys. Rev. Lett. **96**, 167001 (2006).
[16] A. V. Ustinov, M. Cirillo, B. H. Larsen, V. A. Oboznov, P. Carelli, and G. Rotoli, Phys. Rev. B **51**, 3081 (1995).
[17] C. Hutter, A. Shnirman, Y. Makhlin, and G. Schön, Europhys. Lett. **74**, 1088 (2006).
[18] J. Zhang, A. Kamenev, and B. I. Shklovskii, Phys. Rev. Lett. **95**, 148101 (2005).
[19] S. Rachel and A. Shnirman, Phys. Rev. B **80**, 180508(R) (2009).
[20] J. Bonča, S. A. Trugman, and I. Batisti, Phys. Rev. B **60**, 1633 (1999).
[21] S. Coleman, Phys. Rev. D **11**, 2088 (1975).
[22] M. V. Berry, Proc. R. Soc. London A **414**, 31 (1987).